The significance of crack-resistance curves to the mixed-mode fracture toughness of human cortical bone

Elizabeth A. Zimmermann[a,b], Maximilien E. Launey[a] and Robert O. Ritchie[a,b*]

[a] Materials Sciences Division, Lawrence Berkeley National Laboratory, Berkeley, CA 94720

[b] Department of Materials Science and Engineering, University of California, Berkeley, CA 94720

ABSTRACT

The majority of fracture mechanics studies on the toughness of bone have been performed under tensile loading. However, it has recently been shown that the toughness of human cortical bone in the transverse (breaking) orientation is actually much lower in shear (mode II) than in tension (mode I); a fact that is physiologically relevant as *in vivo* bone is invariably loaded multiaxially. Since bone is a material that derives its fracture resistance primarily during crack growth through extrinsic toughening mechanisms, such as crack deflection and bridging, evaluation of its toughness is best achieved through measurements of the crack-resistance or R-curve, which describes the fracture toughness as a function of crack extension. Accordingly, in this study, we attempt to measure for the first time the R-curve fracture toughness of human cortical bone under physiologically relevant mixed-mode loading conditions. We show that the resulting mixed-mode (mode I + II) toughness depends strongly on the crack trajectory and is the result of the competition between the paths of maximum mechanical driving force and "weakest" microstructural resistance.

Keywords: Human cortical bone; mixed-mode fracture; fracture toughness; crack-growth resistance curve

[*]Corresponding author. tel: +1 (510) 486-5798; fax: +1 (510) 643-5792.
E-mail address: roritchie@lbl.gov (R.O. Ritchie).

1. Introduction

Bone fracture is a complex phenomenon that may be understood from the perspective of the multi-dimensional hierarchical nature of the bone-matrix structure [1,2]. Resistance to such bone fracture[1], which is characterized macroscopically by such parameters as the work-of-fracture and the fracture toughness, evolves from a suite of physical structure-related mechanisms that act at multiple length-scales ranging from nano- to near macro-scale dimensions (Fig. 1) [7,8]. These mechanisms can be classified as "plasticity" mechanisms, that operate principally at sub-micrometer dimensions to promote intrinsic toughness (*i.e.*, molecular uncoiling of collagen molecules, fibrillar sliding of both mineralized collagen fibrils and individual collagen fibers, and microcracking), and crack-tip shielding mechanisms, that operate at length-scales of ~1 to 100 μm to promote extrinsic crack-growth toughness (*i.e.*, crack deflection/twist and crack bridging). A central factor of the latter toughening mechanisms is the specific nature of the crack path which is controlled by the applied forces and the nature of the bone-matrix microstructure, in particular the hyper-mineralized interfaces of the osteons (cement lines) (Fig. 2a), which provide microstructurally 'weak', and hence preferred, paths for cracking. As the osteons are aligned nominally along the long axis of the bone, this is the basis of the marked anisotropy in the fracture properties of bone, in that bone is easier to split than to break [9-13] and that the transverse toughness is lower in shear than in tension [10,14,15].

[1]Fracture resistance can be considered as a mutual competition between two classes of mechanisms: *intrinsic* mechanisms, which are microstructural damage mechanisms that operate ahead of the crack tip to promote cracking, and *extrinsic* mechanisms, which operate principally in the wake of the crack tip to inhibit cracking by "shielding" the crack from the applied driving force [3-6]. Whereas intrinsic toughening mechanisms, *e.g.*, plastic deformation, act in general to resist intrinsic microstructural damage and thus are effective in inhibiting both the initiation and growth of cracks, extrinsic toughening mechanisms, *e.g.*, crack bridging, are only effective in inhibiting crack growth [4]..

Fracture mechanics measurements afford the most appropriate methodology to characterize the toughness of bone by providing a quantitative measure of its fracture resistance. However, although bones invariably fracture under complex loading conditions, most measurements to date have involved solely tensile (mode I) loading with linear-elastic fracture mechanics (LEFM) assessments of the K_{Ic} fracture toughness, *i.e.*, the critical value of the mode I stress-intensity factor at the onset of failure[2]. This has been reasoned to be appropriate since, for most materials [16,17], the fracture toughness under mode I (tensile loading) is generally the worst-case. However, recent studies [15] have shown that for human cortical bone in the transverse (breaking) orientation, the fracture toughness in shear is significantly lower than in tension, *i.e.*, the mode I toughness is *not* the worst-case (Fig. 2b). This is significant as physiologically bones are rarely loaded uniaxially and instead are subjected to highly mixed-mode combinations of tension, compression and shear, depending on the character of the applied forces that they experience, the shape of the bone (*i.e.*, how the loads are transferred to a crack), and most notably, the orientation of the crack with respect to the applied loads. Consequently, a more appropriate measure of the fracture resistance of bone must be a mixed-mode fracture toughness comprising contributions from mode I (tensile), mode II (shear), and/or mode III (anti-plane shear) crack displacements (Fig. 3a-c).

Such measurements have recently been made for human cortical bone based on a critical value of the strain-energy release rate, G_c [15], where G is defined in

[2] The stress-intensity factor K characterizes the local distribution of stress and displacement in the vicinity of a sharp crack in a linear-elastic solid. It is determined by $K = Y\sigma_{app}(\pi a)^{1/2}$ where σ_{app} is the applied stress, a is the crack length, and Y is a function (of order unity) of crack size and geometry. Alternatively, the toughness can be expressed in terms of the strain-energy release rate, G, defined as the change in potential energy per unit increase in crack area.

terms of the mode I, II, and III stress intensities (respectively K_I, K_{II}, and K_{III}) as follows:

$$G = \frac{K_I^2}{E'} + \frac{K_{II}^2}{E'} + \frac{K_{III}^2}{2\mu} , \quad (1)$$

where μ is the shear modulus and $E' = E$ (Young's modulus) in plane stress and $E/(1 - \nu^2)$ in plane strain (ν is Poisson's ratio). For the case of modes I and II, the combined mode I tension and mode II shear loading is defined in terms of the phase angle, $\Psi = \tan^{-1}(K_{II}/K_I)$, where K_{II}/K_I is the mode-mixity.

Although evaluating the toughness of bone under more complex loading is an important first step, single-value LEFM toughness parameters based on crack initiation, such as K_{Ic} and G_c, cannot truly capture, or even represent, the multiple length-scale toughening mechanisms (both extrinsic and intrinsic) acting in cortical bone, where the majority of the toughness is derived during crack growth (not crack initiation). As a result, stable (subcritical) cracking precedes outright fracture such that the fracture toughness is better characterized by rising resistance-curve (R-curve) behavior[3], where the fracture resistance actually increases with crack extension.

Accordingly, in this study, we attempt the first resistance-curve characterization of the fracture toughness of human cortical bone under mixed-mode loading conditions, specifically using symmetrical and asymmetrical notched four-point bend testing under combinations of mode I tension and mode II shear (Fig. 3d).

2. Experimental Methods

[3] The crack-resistance or R-curve is a direct result of extrinsic toughening, and as such provides an assessment of the fracture toughness in the presence of subcritical crack growth. It involves measurements of the crack-driving force, *e.g.*, *K*, *G*, or *J*, as a function of crack extension (Δa). The value of the driving force at $\Delta a \rightarrow 0$ provides a measure of the crack-initiation toughness, whereas the slope or the maximum value of the R-curve can be used to characterize the crack-growth toughness.

2.1. Materials

Fresh frozen human cadaveric femurs, from three males aged 48, 52 and 79 years of age, with no known metabolic bone diseases, were used in this study (which was exempt from human subjects authorization because no identifying information was known about the donors). A total of 12 samples were tested in the transverse orientation using notched symmetric and asymmetric four-point bending tests to determine the mode I and mixed-mode fracture toughness, respectively: N=2 from the 48-year-old donor, N=7 from the 52-year–old donor, and N=3 from the 79-year–old donor. The cortical bone, taken from the diaphysis of each femur, was sectioned with an IsoMet 1000 precision low-speed saw (Buehler) into rectangular cross-sectioned beams with a width W ~ 3.1-4.9 mm and a thickness B ~ 2.0-3.4 mm. The samples were notched with a low-speed saw in the transverse (breaking) orientation; in this orientation, the notch is oriented such that the nominal crack-growth direction is from the periosteum to the endosteum and perpendicular to the long axis of the osteons (*out-of-plane* transverse), as shown in Fig. 2a. The notches were sharpened by a micro-notching procedure involving polishing at the root of the notch with a razor blade, which was irrigated with 1-μm diamond suspension, to give a final crack length of a_o ~ 1.8-2.6 mm ($0.41 \leq a_0/W \leq 0.60$) with a reproducible root radius of 3-5 μm. The resulting single-edge notched bend SE(B) specimens were ground with successively finer grit to a 1200 grit finish prior to final polishing with a 1-μm and then a 0.05-μm diamond suspension. All samples were stored in Hanks' Balanced Salt Solution (HBSS) for at least 12 hrs prior to testing.

2.2. Mixed-mode R-curve measurements

The asymmetric four-point bend geometry (Fig. 3d) was used to measure the R-curves under mixed-mode (mode I + II) and pure mode-II ($\Psi = 90°$) conditions, while a pure mode-I loading configuration ($\Psi = 0°$) was achieved by using symmetrical four-point bending (pure bending) of the notched beams. In order to measure the crack growth toughness while simultaneously imaging the initiation and growth of cracks in real time, *in situ* testing of samples soaked in HBSS was performed in a Hitachi S-4300SE/N environmental scanning electron microscope (ESEM) (Hitachi America, Pleasanton, CA) at 25°C using a Gatan Microtest 2-kN four-point bending stage (Gatan, Abington, UK); images of the crack path were obtained simultaneously in back-scattered electron mode at a voltage of 25 kV and a pressure of 35 Pa. Loading was applied under displacement control at a displacement rate of 6.67 μm/s, with an in-house machined rig to apply the asymmetric or symmetric four-point bending load to the sample.

A static equilibrium analysis of the asymmetric four-point bending configuration reveals that a constant shear force, Q, (per unit thickness) is applied to the crack tip along with a moment, M, whose magnitude varies linearly with displacement, c, from the center line of the rig (Fig. 3d):

$$Q = P\frac{y-x}{y+x} \quad \text{and} \quad M = cQ, \tag{2}$$

where P is the applied load, and y and x are the larger and smaller loading spans, respectively, of the rig at which point the load is applied to the sample (Fig. 3d). Accordingly, the phase angle, Ψ, can be tuned by varying the position of the crack with respect to the center line of the rig.

2.3. Stress intensity calculation

A LEFM approach was used to compute crack driving forces. This was justified by the fact that in our experiments, the size of the crack-tip plastic zone,

estimated by $r_y \sim (EG/\sigma_y^2)/2\pi$, where E is Young's modulus (20 GPa) and σ_y is the yield stress (120 MPa), was at least one order of magnitude smaller than the in-plane and out-of-plane dimensions of our fracture test specimens. This ensured that, respectively, a state of small-scale yielding, *i.e.*, K-field dominance, and of plane strain was achieved in these specimens.[4]

For the asymmetric four-point bend geometry, the stress-intensity factors K_I and K_{II} were determined by using the linear-elastic solution that was numerically determined by He and Hutchinson [19], such that:

$$K_I = \frac{6M}{W^2}\sqrt{\pi a}F_I\left(\frac{a}{W}\right) \quad \text{and} \quad K_{II} = \frac{Q}{W^{\frac{1}{2}}}\frac{(a/W)^{\frac{3}{2}}}{(1-a/W)^{\frac{1}{2}}}F_{II}\left(\frac{a}{W}\right). \tag{3}$$

F_I and F_{II}, are the geometry functions tabulated, respectively, in Tada [20] and He and Hutchinson [19], and expressed as follows:

$$F_I\left(\frac{a}{W}\right) = \sqrt{\frac{2W}{\pi a}\tan\frac{\pi a}{2W}}\,\frac{0.923+0.199\left(1-\sin\frac{\pi a}{2W}\right)^4}{\cos\frac{\pi a}{2W}}$$

$$F_{II}\left(\frac{a}{W}\right) = 7.264 - 9.37\left(\frac{a}{W}\right) + 2.74\left(\frac{a}{W}\right)^2 + 1.87\left(\frac{a}{W}\right)^3 - 1.04\left(\frac{a}{W}\right)^4 . \tag{4}$$

In symmetric four-point bending (mode I), the loading configuration creates a region of constant moment between the two inner loading points. Stress-intensity factors can be computed from the standard solution for an edge-cracked plate in pure bending [21], which is equivalent to the solution for K_I in asymmetric loading (Eq. 3), only with a moment of $M = P(S_2 - S_1)/4$, where S_2 and S_1 are the outer and inner loading span, respectively.

[4] A preferred strategy to evaluate the fracture toughness of cortical bone where the extent of local "plasticity" is not small compared to the size of the bone is to use nonlinear elastic fracture mechanics, e.g., J-integral [10,18]. This approach can provide a more realistic description of the crack-tip stress and displacement fields where conditions do not meet the small-scale yielding requirement. Furthermore, the approach can additionally capture the contribution to the toughness from the energy consumed in "plastic" deformation prior to and during fracture. However, J-integral solutions and compliance calibrations, particularly for complex mixed-mode loading and deflected cracks, are far less available compared to the corresponding LEFM solutions.

The asymmetric and symmetric four-point bend stress-intensity solutions are only applicable to coplanar crack growth. If the crack follows a deflected path, the new orientation of the crack tip with respect to the loading changes the stress field and thus, the stress intensities at the crack tip. In order to calculate the stress intensities at the tip of a deflected crack, the asymmetric four-point bending stress intensity solution must be modified. Many numerical solutions exist for determining the local stress intensities at the tip of a deflected crack [22-28] for a very small amount of crack growth. The solution of He and Hutchinson [28], for a kinked crack[5] in a homogeneous material, was chosen for this analysis due to its validity for deflection angles of more than 90° relative to the original crack plane.

To calculate the stress intensity at the tip of a deflected crack, the *global* stress intensities, K_I and K_{II} (see Fig. 4a), were first calculated with the asymmetric four-point bend solution for an equivalent crack of length, a:

$$a = a_o + \Delta a_p, \tag{5}$$

where a_o is the original crack length and Δa_p is equal to the projected length of the growing crack onto the plane of the original crack (Fig. 4a). The *global* stress intensities, K_I and K_{II} (Fig. 4a), were then converted to the *local* stress intensities, k_1 and k_2, effective at the crack tip, by using the following equations, which were numerically derived by He and Hutchinson for a kinked crack in a homogeneous material [28]:

$$k_1 = (c_R + d_R)K_I - (c_I + d_I)K_{II} \ ,$$
$$k_2 = (c_I - d_I)K_I + (c_R - d_R)K_{II} \ , \tag{6}$$

[5] A kinked crack is defined as a semi-finite crack with a small kink at the tip ($\Delta a/a_o \ll 1$).

where c_R, d_R, c_I and d_I are all constants that are tabulated in ref. [29] as a function of the deflection angle, θ (see Fig. 4b), which is the angle of crack deflection with respect to the original crack plane.

2.4. Fracture toughness tests

There are no standards for the fracture toughness testing of bone, nor are there standards for the measurement of the mixed-mode toughness. Although in the current work our focus was on R-curve determination, we nominally followed the procedures of the ASTM E-399 standard for the toughness of metals, specifically based on the determination of stress intensities (as described above) [30]. An alternative ASTM standard (D 5054-99) for the measurement of the plane-strain (mode I) fracture toughness, K_{IC}, developed for plastic materials advises the experimental measurement of strain-energy release rates, G_{IC}, derived from integrating the load-displacement curve [31]. Although we did not use this latter approach in the current work, an indentation and compliance correction can be measured by pressing a pin into an unnotched bone specimen. For our K_C measurements, this so-called indentation-correction (which is not included in the ASTM E-399 standard) was estimated for the current tests to be ~4%, *i.e.*, well less than the coefficient of variability for the fracture toughness of bone which is typically on the order of 20% [32].

2.5.R-curve analysis

To calculate the R-curves, for each increment of crack growth, the stress intensities at the crack tip were calculated, as previously described, in terms of the kinked crack and asymmetric or symmetric four-point bend solutions. To compute a mixed-mode driving force, the strain-energy release rate, G, was

calculated from the *local* mode I and mode II stress intensity factors, k_1 and k_2, at the tip of the kinked crack:

$$G = \frac{k_1^2}{E} + \frac{k_2^2}{E} + \frac{k_3^2}{2\mu} \ , \qquad (7)$$

which is the same form as Eq. 1, with the Young's modulus E = 20 GPa for bone and the mode III component set to zero.

The preferred *mechanically-driven* path of the crack is governed by the direction of the maximum driving force, *i.e.*, a path of maximum G; this is essentially equivalent to a zero phase-angle crack path, governed by $K_{II} = 0$. However, assessing the direction of the driving force during crack growth is a complex calculation. We have estimated the direction of the driving force by first calculating a local phase angle, determined using *local* stress intensities, *i.e.*, $\varphi = \tan^{-1}(k_2/k_1)$, for each increment of the kinked crack; the local phase angle can then be used to determine a kink angle from the numerically based relationship computed by He and Hutchinson [28]. The direction of the driving force is the crack deflection angle minus the kink angle (see Fig. 4b).

3. Results

G-Δa R-curves for the transverse orientation loaded in pure mode I (Ψ = 0°) and at low (Ψ = 12-25°) and high (Ψ = 55-90°) phase angles are shown in Fig. 5. The driving force-crack extension data are replotted in Fig. 6 as three-dimensional R-curves, where the third axis is the phase angle, Ψ.

3.1. Pure Mode I R-curve

For the transverse orientation loaded in mode I, the preferred mechanical (G_{max}) crack path and preferred microstructural crack paths (along the cement lines) are initially perpendicular. The crack begins to extend when the applied

driving force exceeds the crack-initiation toughness[6]; with subsequent (subcritical) crack extension over several hundred micrometers, an increased applied driving force is required to sustain cracking (Fig. 5a) due to the creation of extrinsic toughening mechanisms, such as crack deflection and bridging, with crack growth. The crack-growth toughness can be defined by a linear fit to the slope of the R-curve, and ranges in this orientation from 0.43 to 2.39 J/m^2/μm in mode I. Thus, the toughness of bone increases as the crack advances with an increasing driving force required to cause further extension. Even though there are sample-to-sample variations in the magnitude and shape of the R-curves, the toughness of the bone exceeds G = 200 J/m^2 after at least 200 μm of crack growth.

Similarly in Fig. 7, sample R-curves are shown with an image of their final crack length; the amount of crack extension at each increment of crack growth is marked with a dotted blue line, while the direction of the driving force is indicated in orange. As the crack advances in mode I, the driving force remains perpendicular to the preferred microstructural direction (Fig. 7a), *i.e.*, the preferred direction of the mechanical (G_{max}) path remains parallel to the original crack, even though the crack deflects out of the original crack plane (shown by the deflection angle, θ, in Fig. 7a). When the preferred direction of the mechanical driving force is perpendicular to the preferred microstructural path, the process of such crack deflection acts as a potent toughening mechanism because it leads to a reduction in the stress intensity locally experienced at the crack tip; for a mode I crack subject to a simple in-plane deflection of 90°, the local stress is reduced by roughly 50% [23,27]. Thus, the bone-matrix microstructure regulates the crack path by causing crack deflections principally

[6] The initial point on the R-curve, the crack-initiation toughness, is often difficult to measure as its value depends critically on the nature and especially the sharpness of the pre-crack (or micro-notch) from which fracture ensues. However, the small number of data points collected in this study does not allow for an accurate measure of the initiation toughness to be made.

at cement lines [10], which in turn results in an increase in the toughness with crack extension, *i.e.*, rising R-curve behavior; the toughness is further enhanced as the number of deflections or their severity increases. Thus, the highest toughness will be measured for cracks that deflect along the preferred microstructural path, while the G_{max} direction remains constant (0° from the original crack plane).

3.2. Pure Mode-II R-curves

In mode II, the direction of the mechanical driving force (~74° from the original crack plane) and the direction of the preferred microstructural path (~90° from the original crack plane) are nearly commensurate before crack extension begins (consistent with the low toughness of bone in shear). The crack-growth toughness for subsequent crack extension over several hundred micrometers was 0.33 J/m^2/μm (Fig. 5c) for both mode-II R-curves. Thus, akin to mode I, the toughness increases with crack extension but to a smaller extent. Even though the toughness in mode II does increase by a factor of two over ~ 50 - 150 μm in crack growth, the maximum toughness never exceeds G = 80 J/m^2. Thus, in mode II, the onset of outright fracture or instability, *i.e.,* unstable cracking, is reached faster than mode I because the R-curves are shallower, as clearly shown in the three-dimensional R-curves plotted in Fig. 6.

The reason why bone has a lower toughness in shear (mode II) can be understood by examining the direction of the maximum mechanical driving force with crack extension (Fig. 7c). As the crack extends, the G_{max} direction remains nearly constant at 74°, *i.e.,* the crack tip remains loaded in shear; thus, the direction of the driving force at the crack tip remains nearly commensurate with the preferred microstructural path. The path that the crack takes, *i.e.*, the deflection angle θ (Fig. 7c), is nearly parallel to the preferred microstructural

path. Under these conditions, bone will display a low toughness since the crack will have no impediment to following the path of lowest microstructural resistance because the preferred microstructural and mechanical paths are aligned. There is little motivation for the crack to deflect (with respect to the G_{max} direction), while correspondingly the fracture surfaces are comparatively smooth, which is consistent with the low toughness and shallower R-curves.

The toughness still increases with crack growth in mode II. However, as described in detail in refs. [10,15], where the preferred mechanical and microstructural paths are aligned, extrinsic toughening in bone results primarily from the formation of (typically cement line) microcracks that form ahead and parallel to the main growing crack. The intact regions in between can then act as bridging ligaments, so called "uncracked-ligament" bridging (Figs. 7c, 8), which can toughen the material by carrying load that would otherwise be used to promote further crack extension. This mechanism, however, is considerably less potent than the crack deflection mechanisms described above [10].

3.3. Mixed-mode I-II R-curves

Under mixed-mode loading, prior to crack extension, the direction of the maximum driving force is at an angle between 0° and 74° (depending on the applied mode-mixity) to the original crack plane. As the crack extends, the required driving force for the next increment of crack growth increases (Fig. 5b,c), leading to rising R-curve behavior, as in pure mode I and mode II. As might be expected, the competition between the preferred mechanical and microstructural paths results in toughness values that are intermediate between the high mode I values and the low mode II values (Fig. 6).

The cause of this behavior is fairly complicated and may likely vary for each sample depending on microstructural variations ahead of the crack tip.

However, *in situ* observations in the SEM indicated two different modes of behavior. At one extreme, the deflection angle remained roughly constant, *i.e.*, the crack path followed the preferred microstructural direction (90° deflection), while the path of maximum G diverged from the crack path. Thus, crack deflection here causes significant increases in the toughness with crack growth. As this divergence is never as great as in pure mode I, the R-curves are not as steep. SEM micrographs of the crack path (for Ψ = 13° in Fig. 7b) show a combination of toughening mechanisms in the form of crack deflection and uncracked-ligament bridging.

At the other extreme, the direction of the maximum driving force remained constant while the deflection angle changed. In this case, the crack path becomes increasingly dominated by the preferred microstructural direction (see Ψ = 16° in Fig. 7b). Again the preferred directions become increasingly divergent with crack extension, although now the salient toughening mechanism appears to be solely crack deflection.

4. Discussion

In vivo, bones invariably break under mixed-mode loading with often complicated fracture patterns. The central hypothesis of this work is that the variation in cortical bone toughness with loading mode can be interpreted in terms of the fracture path, specifically in terms of the competition between the preferred mechanical and microstructural crack paths. The preferred microstructural crack path is along the cement lines, *i.e.*, along the long axis of the bone (Fig. 2a), which in the transverse orientation is perpendicular to the original crack plane; the preferred mechanical crack path is the path of the maximum driving force, *i.e.*, the direction of maximum G, which varies between 0° and 74° with respect to the original crack plane for mode I and mode II,

respectively [28]. For the toughness of human cortical bone in the transverse orientation (Fig. 2b), a consideration of these crack paths clearly shows why bone displays a higher toughness in tension (Mode I) than in shear (Mode II) [15], which at first glance is a surprising result.

In mode I tension, the transverse toughness of human cortical bone increases with crack extension because the preferred mechanical (G_{max}) path remains orthogonal to the preferred microstructural path, which is along the long axis of the bone (Fig. 7a). When this occurs, a progressively higher driving force is required for further crack extension, *i.e.*, due to crack deflections in mode I the toughness of the material increases. This is manifest as the steepest R-curves for any mode-mixity, consistent with the highly deflected crack paths and rough fracture surfaces [15]. Since the bending of bones perpendicular to their long axis would be deemed the most severe form of loading, Nature has clearly designed bone to be most fracture resistant in this orientation.

In mode II (in-plane) shear, the direction of the driving force and the preferred microstructural path are nearly identical (Fig. 7c) as the crack propagates. Consequently, the crack is able to nominally follow the preferred microstructural path since the driving force is nearly aligned with this path; deflection is therefore limited and will not be a significant source of toughening. As microcracks now tend to form ahead and parallel to the growing crack, the primary source of toughening is crack bridging, with relatively linear crack paths and planar fracture surfaces (Fig. 8). In addition, the R-curves tend to be shallowest in this mode (Fig. 6). Clearly, because of this, cortical bone is less resistant to fracture in shear. Cracks can propagate in the shear-like mode that is associated with the linking of nominally parallel microcracks (Fig. 8); these shear cracks closely resemble the *en echelon* cracks associated with earthquake faults in rocks [33,34] (which, like bone, is also a microcracking solid).

Under mixed-mode tension and shear loads, cracks appear to follow a path that leads to an increasing divergence between the preferred mechanical and microstructural paths. However, as this divergence is invariably less than in mode I, R-curves are steeper than in mode II but less so than in mode I. Under these conditions, both primary toughening mechanisms, *i.e.*, crack deflection and uncracked-ligament bridging, prevail.

5. Conclusions

Based on an analysis of mixed-mode fracture and crack growth in transversely oriented human cortical bone, the following conclusions can be made.

1. The toughness of bone results from a competition between the direction of the paths of maximum mechanical driving force (G_{max}) and weakest microstructural resistance (along the cement lines parallel to the long axis of the bone). When these directions are commensurate, bone has a low crack growth toughness; when they are divergent, these fracture toughness values become significantly enhanced.
2. The toughness of bone is highest under pure mode I tensile loading where the preferred microstructural and mechanical paths are most divergent. The competition between these two paths leads to significant crack deflection, which provides the main source of toughening. As the driving force remains coplanar with the original crack after the crack deflects, a larger driving force is required to sustain cracking; R-curves are thus steepest in this loading mode, resulting in the highest crack growth toughness.

3. The toughness of bone is lowest under pure mode II (in-plane) shear loading where the preferred microstructural and mechanical paths are more closely aligned. Under these conditions, the toughness associated with crack extension is correspondingly much lower and does not increase as significantly with crack extension. Crack paths are thus relatively linear and toughening is associated with crack bridging resulting from the formation of microcracks ahead or parallel to the main growing crack.
4. Under mixed-mode tension and shear loading, the toughness still increases with crack extension due to a progressive divergence of the preferred microstructural and mechanical crack paths. Toughness values, however, are intermediate between those measured in pure mode I and mode II, with toughening associated with both crack deflection and crack bridging.

Acknowledgements

This work was supported by the National Institute of Health (NIH/NIDCR) under grant No. 5R01 DE015633 through the U.S. Department of Energy under contract No. DE-AC02-05CH11231. The authors wish to thank Dr. Tony P. Tomsia, at the Lawrence Berkeley National Laboratory, for many helpful discussions and Professor Tony M. Keaveny and Mike Jekir, of the Mechanical Engineering Department at the University of California, Berkeley, for graciously allowing us to use their facilities to machine samples for this project.

References

[1] Weiner S, Wagner HD. The material bone: Structure mechanical function relations. Annu. Rev. Mater. Sci. 1998;28:271.

[2] Fratzl P, Weinkamer R. Nature's hierarchical materials. Prog. Mater. Sci. 2007;52:1263.

[3] Evans AG. Perspective on the development of high-toughness ceramics. J. Am. Ceram. Soc. 1990;73:187.

[4] Ritchie RO. Mechanisms of fatigue crack-propagation in metals, ceramics and composites: role of crack tip shielding. Mater. Sci. Eng., A 1988;103:15.

[5] Launey ME, Ritchie RO. On the fracture toughness of advanced materials. Adv. Mater. 2009;21:2103.

[6] Ritchie RO. Mechanisms of fatigue-crack propagation in ductile and brittle solids. Int. J. Fract. 1999;100:55.

[7] Launey ME, Buehler MJ, Ritchie RO. On the mechanistic origins of toughness in bone. Ann Rev Mater Res 2010;40:9.1.

[8] Ritchie RO, Buehler MJ, Hansma PK. Plasticity and toughness in bone. Phys Today 2009;62:41.

[9] Nalla RK, Kinney JH, Ritchie RO. Mechanistic fracture criteria for the failure of human cortical bone. Nat. Mater. 2003;2:164.

[10] Koester KJ, Ager JW, Ritchie RO. The true toughness of human cortical bone measured with realistically short cracks. Nat. Mater. 2008;7:672.

[11] Yeni YN, Norman TL. Calculation of porosity and osteonal cement line effects on the effective fracture toughness of cortical bone in longitudinal crack growth. J. Biomed. Mater. Res. 2000;51:504.

[12] Peterlik H, Roschger P, Klaushofer K, Fratzl P. From brittle to ductile fracture of bone. Nat. Mater. 2006;5:52.

[13] Yeni YN, Fyhrie DP. A rate-dependent microcrack-bridging model that can explain the strain rate dependency of cortical bone apparent yield strength. J. Biomech. 2003;36:1343.

[14] Nalla RK, Stolken JS, Kinney JH, Ritchie RO. Fracture in human cortical bone: local fracture criteria and toughening mechanisms. J. Biomech. 2005;38:1517.

[15] Zimmermann EA, Launey ME, Barth HB, Ritchie RO. Mixed-mode fracture of human cortical bone. Biomaterials 2009;30:5877.

[16] Singh D, Shetty DK. Fracture toughness of polycrystalline ceramics in combined mode I and mode II loading. J. Am. Ceram. Soc. 1989;72:78.

[17] He MY, Cao HC, Evans AG. Mixed-mode fracture: The four-point bending shear specimen. Acta Metall. Mater. 1990;38:839.

[18] Launey ME, Chen PY, McKittrick J, Ritchie RO. Mechanistic aspects of the fracture toughness of elk antler bone. Acta Biomater. 2010;6:1505.

[19] He MY, Hutchinson JW. Asymmetric four-point crack specimen. J. Appl. Mech.-Trans. ASME 2000;67:207.

[20] Tada H, Paris PC, Irwin GR. The Stress Analysis of Cracks Handbook. St. Louis, MO, USA.: Paris Production Inc., 1985.

[21] Anderson TL. Fracture Mechanics: Fundamentals and Applications. 3rd. Ed., Boca Raton, FL: Taylor and Francis Group, 2005.

[22] Kitagawa H, Yuuki R, Ohira T. Crack-morphological aspects in fracture mechanics. Eng. Fract. Mech. 1975;7:515.

[23] Cotterell B, Rice JR. Slightly curved or kinked cracks. Int. J. Fract. 1980;16:155.

[24] Lo KK. Analysis of branched cracks. J. Appl. Mech.-Trans. ASME 1978;45:797.

[25] Karihaloo BL, Keer LM, Nemat Nasser S. Crack kinking under nonsymmetric loading. Eng. Fract. Mech. 1980;13:879.

[26] Chatterjee SN. The stress field in the neighbourhood of a branched crack in an infinite elastic sheet. International Journal of Solids and Structures 1975;11:521.

[27] Bilby BA, Cardew GE, Howard IC. Stress intensity factors at the tips of kinked and forked cracks. The Fourth International Conference on Fracture, vol. 3A: Pergamon Press, New York, 1978. p.197.

[28] He MY, Hutchinson JW. Kinking of a crack out of an interface. J. Appl. Mech. 1989;56:270.

[29] He MY, Hutchinson JW. Kinking of a crack out of an interface: Tabulated solution coefficients. Cambridge, MA: Harvard University Report MECH-113A, 1989.

[30] ASTM Standard E-399. Standard test method for linear-elastic plane-strain fracture toughness K_{IC} of metallic materials. West Conshohocken, PA: American Society for Testing and Materials, 2006.

[31] ASTM Standard D 5054-99. Standard test methods for plane-strain fracture toughness and strain energy release rate of plastic materials. West Conshohocken, PA: American Society for Testing and Materials, 2007.

[32] Ritchie RO, Koester KJ, Ionova S, Yao W, Lane NE, Ager JW. Measurement of the toughness of bone: A tutorial with special reference to small animal studies. Bone 2008;43:798.

[33] Peng S, Johnson AM. Crack growth and faulting in cylindrical specimens of Chelmsford granite. Int. J. Rock Mech. Min. Sci. 1972;9:37.

[34] Etchecopar A, Granier T, Larroque JM. Origin of en echelon cracks: Propagation of faults. C. R. Acad. Sci., Ser. II 1986;302:479.

[35] Norman TL, Nivargikar SV, Burr DB. Resistance to crack growth in human cortical bone is greater in shear than in tension. J. Biomech. 1996;29:1023.

[36] Jernkvist LO. Fracture of wood under mixed mode loading II. Experimental investigation of Picea abies. Eng. Fract. Mech. 2001;68:565.

List of Figure Captions

Fig. 1. The structure of bone showing the seven levels of hierarchy with the prevailing toughening mechanisms. At the smallest level, at the scale of the tropocollagen molecules and mineralized collagen fibrils, (intrinsic) toughening, *i.e.*, plasticity, is achieved via the mechanisms of molecular uncoiling and intermolecular sliding of molecules. At coarser levels at the scale of the fibril arrays, microcracking and fibrillar sliding act as plasticity mechanisms and contribute to the intrinsic toughness. At micrometer dimensions, the breaking of sacrificial bonds at the interfaces of fibril arrays contributes to increased energy dissipation, together with crack bridging by collagen fibrils. At the largest length-scales in the range of 10s to 100s μm, the primary sources of toughening are extrinsic and result from extensive crack deflection and crack bridging by uncracked ligaments, both mechanisms that are motivated by the occurrence of microcracking. (Adapted from refs. [7 8]).

Fig. 2. (a) A schematic of the cortical bone in a human femur. The secondary osteons are generally oriented parallel to the long axis of the bone, while the cement lines are located at the boundaries of the secondary osteons. The samples in this study were oriented in the transverse orientation (L-R)*, such that the original crack plane was perpendicular to the orientation of the osteons. (b) The critical strain-energy release rate, *i.e.*, toughness, of bone under mixed-mode conditions, is highly dependent on the orientation. In the transverse orientation (L-R), bone has a higher toughness in tension (mode I), while a preliminary analysis of the longitudinal orientation (C-L) suggests an opposite trend [15,35]. The latter behavior, with the mode I toughness as worst-case, is the commonly observed behavior for most brittle materials, as shown here for longitudinally

oriented wood [36], alumina [16], and zirconia [16]. The G_c toughness values are normalized by the worst-case toughness G_o, which is, respectively, the mode-I fracture toughness G_{Ic} values in the case of the longitudinally oriented bone and wood, alumina, and zirconia, and the mode II toughness, G_{IIc}, for transversely oriented bone. (*The first letter in the designation refers to the normal direction to the crack plane, whereas the second letter refers to the expected direction of crack propagation. L stands for the longitudinal direction, C stands for the circumferential direction, and R stands for the radial direction.)

Fig. 3. Cracks can be subjected to (a) mode I (tensile opening), (b) mode II (in-plane shear), or (c) mode III (out-of-plane shear) loading conditions, or combinations of the three. (d) The asymmetric four-point bending geometry applies an asymmetric mixed-mode I-II load to the crack tip. When the crack tip is directly underneath the load, P, which is applied along the centerline of the sample, the sample is in mode II. As the distance of the crack tip from the centerline of the sample increases, the mode I component of the applied load increases. For mode I, a symmetric four-point bending geometry was used.

Fig. 4. (a) A magnified view of the crack tip shows that when the crack deflects with respect to the original plane of the crack, local stress intensities (k_1 and k_2) arise at the crack tip; the local k's are derived from the global stress intensities (K_I and K_{II}) via a kinked-crack solution. The global stress intensities are calculated with the asymmetric four-point bend solution for a crack with length $a = a_o + \Delta a_p$, which is the length of the kinked crack projected onto the original crack plane. (b) When an asymmetric load is applied, the crack deflects at an angle θ from the original crack plane. The direction of the G_{max} path at each increment of crack

growth is assessed from the local stress intensities using the analysis of He and Hutchinson [28].

Fig. 5. Traditional two-dimensional R-curves for human cortical bone in the transverse orientation loaded in (a) mode I ($\Psi = 0°$), (b) at low phase angles (Ψ = 12-25°), and (c) at high phase angles (Ψ = 55-90°). The resistance of the material is measured in terms of the strain energy release rate and given as a function of crack extension. As R-curves for the tensile opening case have shown, bone exhibits stable crack extension in combined mode I-II loading [10]. The occurrence of a rising R-curve thus indicates that as the crack grows, a larger driving force is needed for crack extension. At higher phase angles, the R-curve is shallower because the paths of maximum mechanical driving force and the preferred microstructural paths (generally along the cement lines) are more closely aligned, which encourages crack deflection along the brittle interfaces in the microstructure.

Fig. 6. Three-dimensional R-curves for transverse-orientated human cortical bone obtained by plotting the two-dimensional R-curves from Fig. 5 together with an additional axis that represents the phase angle, Ψ. The marked decrease in the fracture resistance of the material with crack growth can be seen as the amount of mode II loading (phase angle) increases. The dotted lines are the projections of the three-dimensional lines onto the Ψ-Δa axis.

Fig. 7. Two-dimensional R-curves for the (a) mode I, (b) mixed-mode, and (c) mode II samples of transverse-orientated human cortical bone along with an image of the crack extension. The dotted red line indicates the initial crack position, the dotted blue lines indicate the increments of crack growth, and the

orange line indicates the G_{max} direction at that position. With respect to the comparison between the G_{max} direction and the actual crack path, higher toughness values result when the driving force is perpendicular to the weak microstructural path.

Fig. 8. Crack bridging in human cortical bone for a crack loaded in shear (mode II). The crack follows the preferred microstructural path, which is perpendicular to the original plane of the crack. Such apparent shear cracks propagate in a fashion very similar to *en echelon* cracks associated with earthquake faults in microcracking rocks.

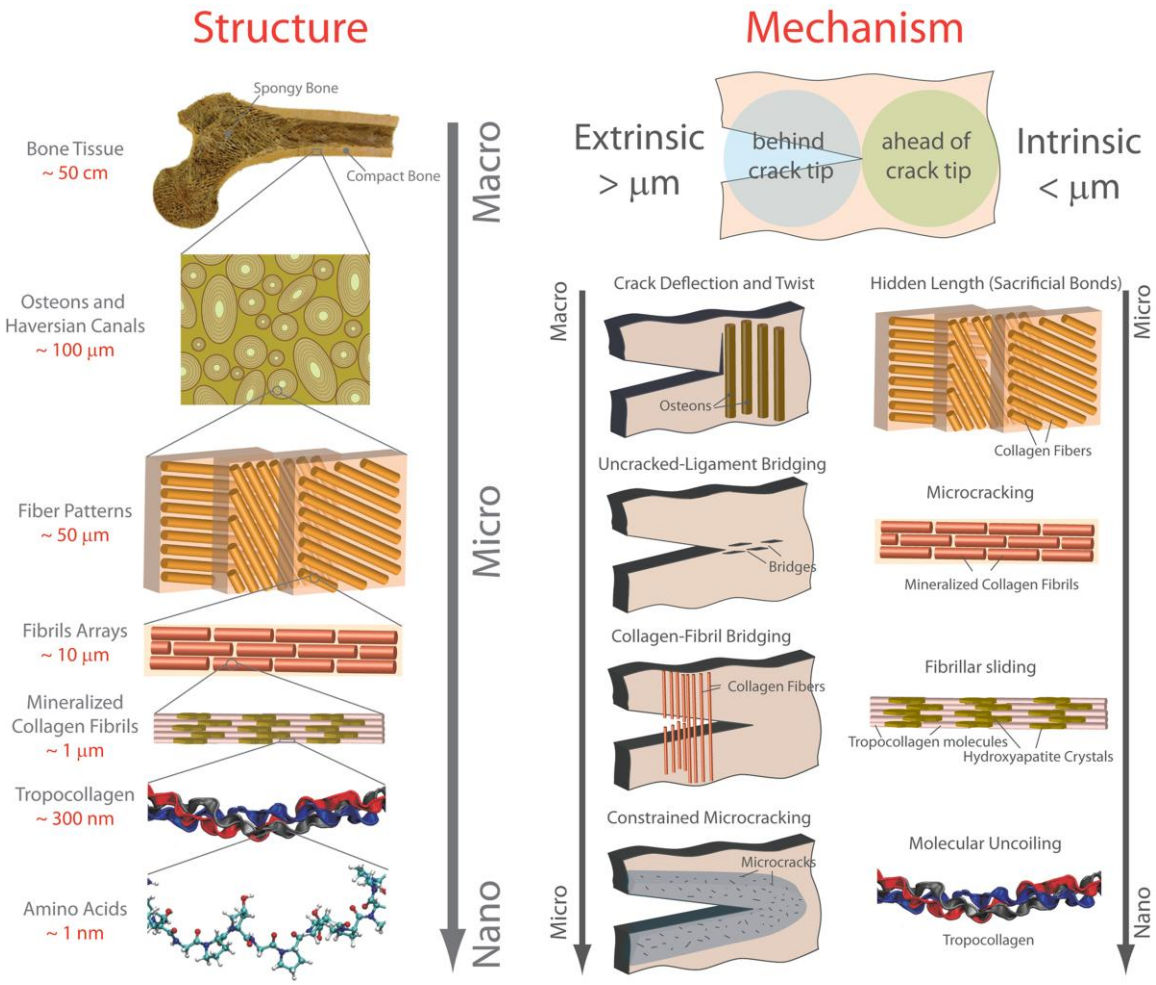

Fig. 1. The structure of bone showing the seven levels of hierarchy with the prevailing toughening mechanisms. At the smallest level, at the scale of the tropocollagen molecules and mineralized collagen fibrils, (intrinsic) toughening, *i.e.*, plasticity, is achieved via the mechanisms of molecular uncoiling and intermolecular sliding of molecules. At coarser levels at the scale of the fibril arrays, microcracking and fibrillar sliding act as plasticity mechanisms and contribute to the intrinsic toughness. At micrometer dimensions, the breaking of sacrificial bonds at the interfaces of fibril arrays contributes to increased energy dissipation, together with crack bridging by collagen fibrils. At the largest length-scales in the range of 10s to 100s µm, the primary sources of toughening are extrinsic and result from extensive crack deflection and crack bridging by uncracked ligaments, both mechanisms that are motivated by the occurrence of microcracking. (Adapted from refs. [7,8]).

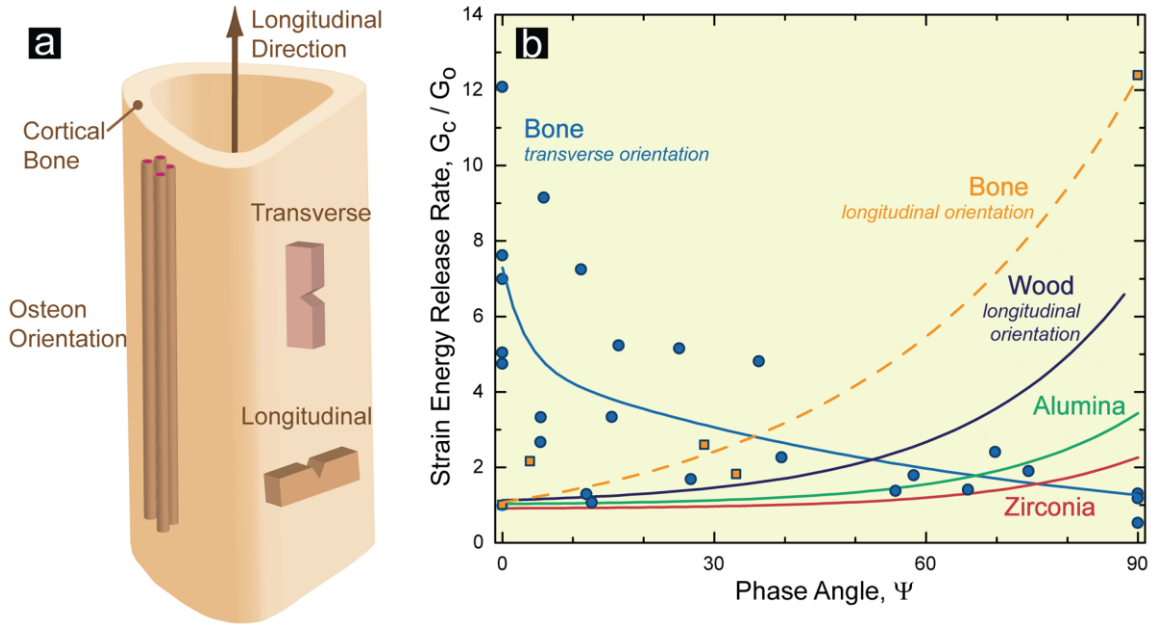

Fig. 2. (a) A schematic of the cortical bone in a human femur. The secondary osteons are generally oriented parallel to the long axis of the bone, while the cement lines are located at the boundaries of the secondary osteons. The samples in this study were oriented in the transverse orientation (L-R)*, such that the original crack plane was perpendicular to the orientation of the osteons. (b) The critical strain-energy release rate, *i.e.*, toughness, of bone under mixed-mode conditions, is highly dependent on the orientation. In the transverse orientation (L-R), bone has a higher toughness in tension (mode I), while a preliminary analysis of the longitudinal orientation (C-L) suggests an opposite trend [15,35]. The latter behavior, with the mode I toughness as worst-case, is the commonly observed behavior for most brittle materials, as shown here for longitudinally oriented wood [36], alumina [16], and zirconia [16]. The G_c toughness values are normalized by the worst-case toughness G_o, which is, respectively, the mode-I fracture toughness G_{Ic} values in the case of the longitudinally oriented bone and wood, alumina, and zirconia, and the mode II toughness, G_{IIc}, for transversely oriented bone. (*The first letter in the designation refers to the normal direction to the crack plane, whereas the second letter refers to the expected direction of crack propagation. L stands for the longitudinal direction, C stands for the circumferential direction, and R stands for the radial direction.)

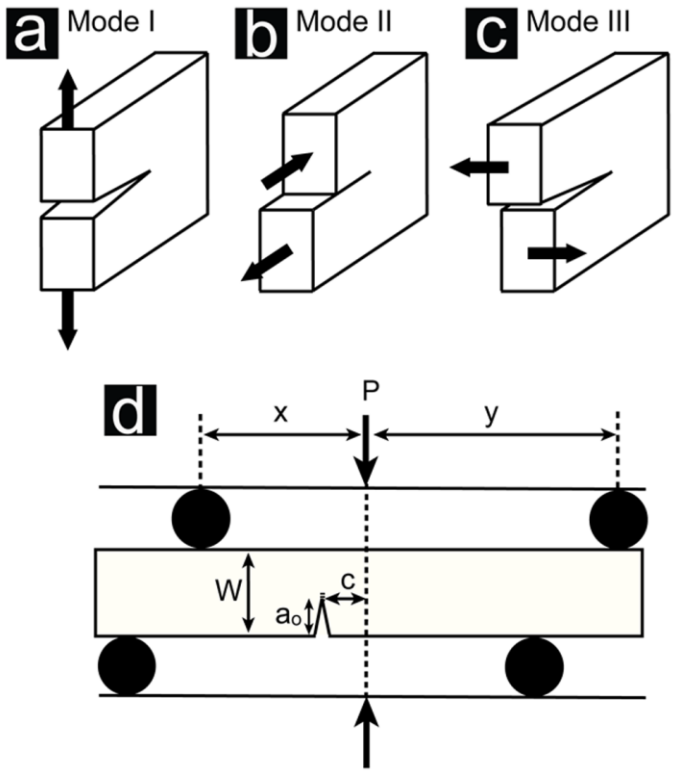

Fig. 3. Cracks can be subjected to (a) mode I (tensile opening), (b) mode II (in-plane shear), or (c) mode III (out-of-plane shear) loading conditions, or combinations of the three. (d) The asymmetric four-point bending geometry applies an asymmetric mixed-mode I-II load to the crack tip. When the crack tip is directly underneath the load, *P*, which is applied along the centerline of the sample, the sample is in mode II. As the distance of the crack tip from the centerline of the sample increases, the mode I component of the applied load increases. For mode I, a symmetric four-point bending geometry was used.

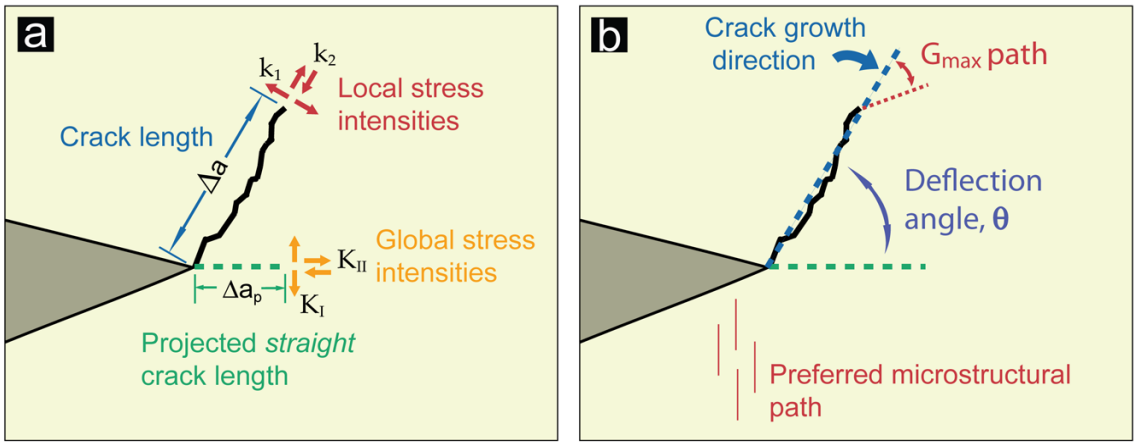

Fig. 4. (a) A magnified view of the crack tip shows that when the crack deflects with respect to the original plane of the crack, local stress intensities (k_1 and k_2) arise at the crack tip; the local k's are derived from the global stress intensities (K_I and K_{II}) via a kinked-crack solution. The global stress intensities are calculated with the asymmetric four-point bend solution for a crack with length $a = a_o + \Delta a_p$, which is the length of the kinked crack projected onto the original crack plane. (b) When an asymmetric load is applied, the crack deflects at an angle θ from the original crack plane. The direction of the G_{max} path at each increment of crack growth is assessed from the local stress intensities using the analysis of He and Hutchinson [28].

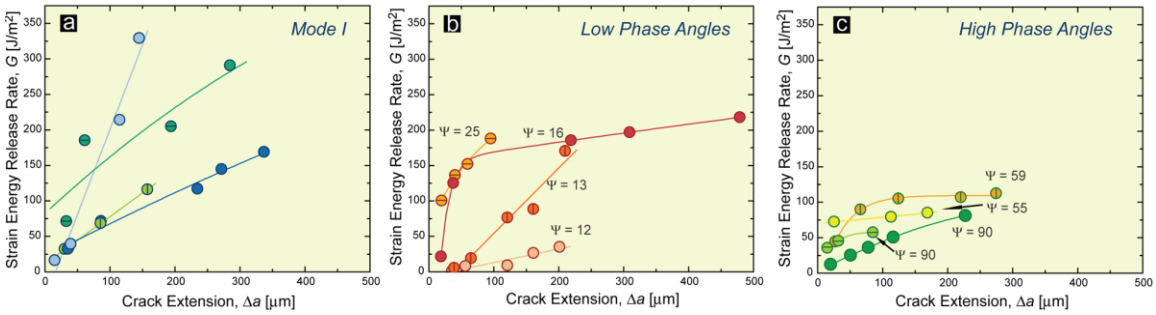

Fig. 5. Traditional two-dimensional R-curves for human cortical bone in the transverse orientation loaded in (a) mode I (Ψ = 0°), (b) at low phase angles (Ψ = 12-25°), and (c) at high phase angles (Ψ = 55-90°). The resistance of the material is measured in terms of the strain energy release rate and given as a function of crack extension. As R-curves for the tensile opening case have shown, bone exhibits stable crack extension in combined mode I-II loading [10]. The occurrence of a rising R-curve thus indicates that as the crack grows, a larger driving force is needed for crack extension. At higher phase angles, the R-curve is shallower because the paths of maximum mechanical driving force and the preferred microstructural paths (generally along the cement lines) are more closely aligned, which encourages crack deflection along the brittle interfaces in the microstructure.

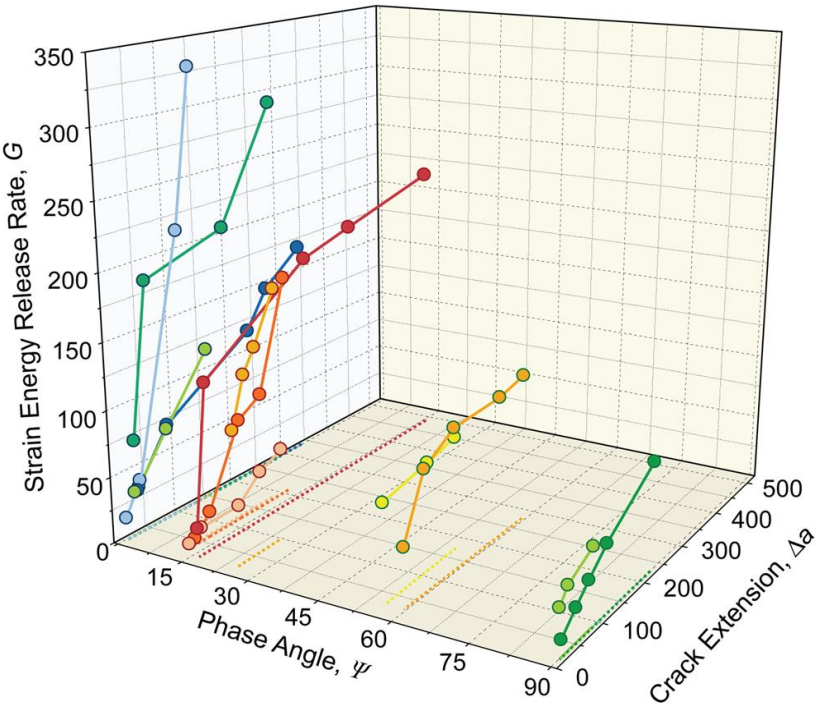

Fig. 6. Three-dimensional R-curves for transverse-orientated human cortical bone obtained by plotting the two-dimensional R-curves from Fig. 5 together with an additional axis that represents the phase angle, Ψ. The marked decrease in the fracture resistance of the material with crack growth can be seen as the amount of mode II loading (phase angle) increases. The dotted lines are the projections of the three-dimensional lines onto the Ψ-Δ*a* axis.

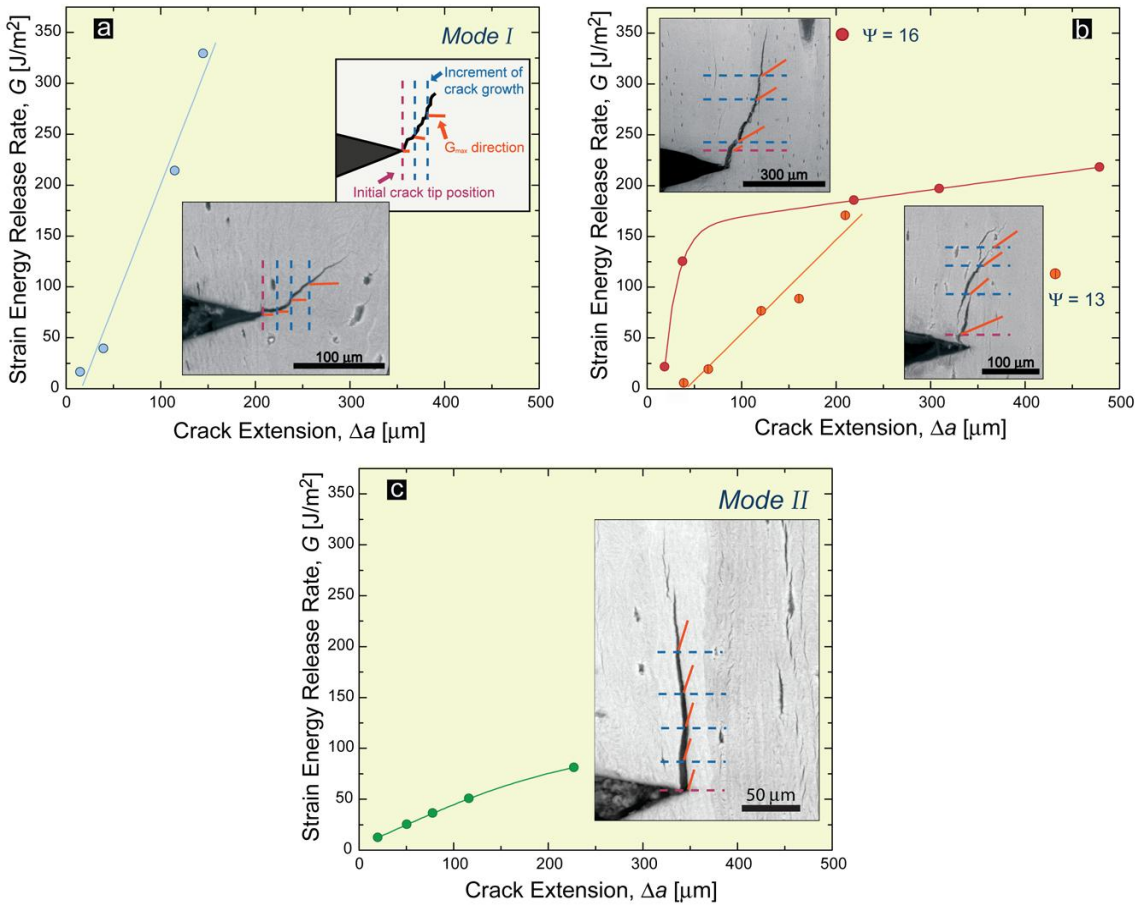

Fig. 7. Two-dimensional R-curves for the (a) mode I, (b) mixed-mode, and (c) mode II samples of transverse-orientated human cortical bone along with an image of the crack extension. The dotted red line indicates the initial crack position, the dotted blue lines indicate the increments of crack growth, and the orange line indicates the G_{max} direction at that position. With respect to the comparison between the G_{max} direction and the actual crack path, higher toughness values result when the driving force is perpendicular to the weak microstructural path.

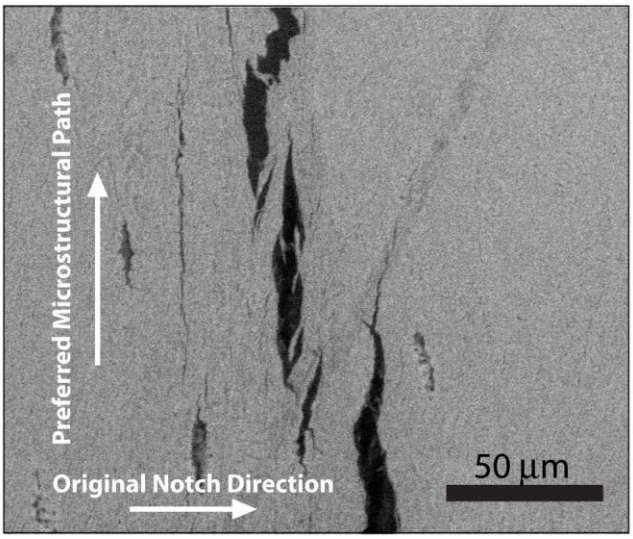

Fig. 8. Crack bridging in human cortical bone for a crack loaded in shear (mode II). The crack follows the preferred microstructural path, which is perpendicular to the original plane of the crack. Such apparent shear cracks propagate in a fashion very similar to *en echelon* cracks associated with earthquake faults in microcracking rocks.